Quantifying Hydrodynamic Trade-Offs in Regeneration: Four-Quadrant Mapping for Sailing-Yacht Propulsors

Hamdi Sena Nomak
Department of Maritime Transportation Engineering, Istanbul Technical University, Turkiye
nomak@itu.edu.tr (corresponding author)

Ismail Cicek
Department of Marine Engineering, Istanbul Technical University, Turkiye
cicekism@itu.edu.tr

Received: 14 September 2025 | Revised: 15 October 2025 and 19 October 2025 | Accepted: 21 October 2025

 DOI: https://doi.org/10.48084/etasr.14789

ABSTRACT

This study investigates the hydrodynamic feasibility of integrating regenerative hydro-turbines into a 12 m sailing yacht, as part of a zero-emission propulsion system. A custom two-bladed propeller was designed using systematic series methods, lifting-surface analysis, and validated Reynolds-Averaged Navier-Stokes (RANS) Computational Fluid Dynamics (CFD) simulations. The propeller achieved ~54% open-water efficiency at the 6 kn, 6 kW design point, meeting thrust requirements while also reducing drag in free-wheeling mode. Two hydro-turbines added only 9-10% resistance across 3-7 kn. In generating mode, each turbine produced 200-300 W under a thrust load of 5-6 kn, with a manageable speed loss of approximately 0.3 kn. This performance enables continuous charging during passages. Despite the increasing use of hydro-generators in practice, yacht-scale hydrodynamic data coupling four-quadrant propeller behavior with hull resistance remain scarce. Prior studies have optimized propellers or turbines in isolation, but few have quantified the net energy-drag trade-off in realistic sailing conditions. The current study fills this gap by producing yacht-scale four-quadrant KT-KQ-J maps with turbine operation, integrating them into validated hull resistance models, and deriving non-dimensional "net-energy-versus-drag" charts. The results provide actionable guidance on when regeneration yields net benefit, offering designers and operators a framework for practical, performance-optimized deployment of regenerative systems in sustainable yacht design.

Keywords-hydrodynamics; hydro-turbines; regeneration; four quadrant hydrodynamic mapping

I. INTRODUCTION

Marine transportation is a great source of greenhouse gas emissions, prompting urgent decarbonization. Although recreational yachts contribute only a small share, their sheer number means adopting wind-assisted or electric propulsion [1] could still significantly reduce emissions. Sailing yachts achieve near-zero emissions via wind power but rely on diesel engines for auxiliary needs (navigation, communication, and amenities), undermining these gains and highlighting the need for renewable onboard power. Consequently, many diesel-dependent yachts are being retrofitted with hybrid or fully electric systems to cut carbon output. For instance, a Philippine analysis in [2] identified over 9,200 small vessels suitable for electrification, a step that could cut maritime CO_2 emissions by about 22%, illustrating the benefits of renewable energy in yacht propulsion.

Hydro-generation provides a viable path to renewable onboard power by converting the flow around a moving hull into electricity. On sailing yachts, this is realized either by operating the main propeller in turbine mode or by deploying dedicated hydro-turbines. In both cases, the vessel's forward motion drives the rotor, generating electricity to reduce reliance on diesel generators, lower fuel costs, and cut greenhouse gas emissions, directly meeting "green yachting" objectives. Authors in [3] confirmed its potential by demonstrating regenerative propeller braking on naval vessels to stabilize power demand, effectively turning the propeller into a flywheel generator. Although developed for warships, the principle directly applies to sailing yachts, where the propulsor can act simultaneously as a propulsion device and an energy harvester.

The main engineering challenge lies in balancing power generation against hydrodynamic performance. Extracting energy inevitably increases resistance, diverting part of the sail's propulsive force into electricity at the expense of speed. Authors in [4] highlighted this equilibrium: as speed rises, the turbine output increases and so does drag, until the system stabilizes at a reduced velocity. Dual-mode devices, thus,

require multi-objective optimization to maximize the net benefit, delivering meaningful electrical output while minimizing the penalties in speed, stability, and trim.

Advances in yacht propulsion meet these goals. Modern yachts employ variable-geometry propellers, such as feathering or folding types, that minimize drag when idle. These are now adapted for dual use, operating as efficient propulsors under engine power and as turbines under sail. Examples include the SAIL-POD system, a four-bladed folding propeller validated in towing tanks, as well as Gori Propeller's hybrid folding design with a hydrogeneration mode. Such innovations demonstrate that regenerative systems are no longer experimental but are increasingly practical with today's technology.

Authors in [5] showed that standard pumps can operate in reverse as micro-hydro turbines, generating 5–1000 kW at ~70% efficiency. Sailing yachts already deploy trailing or hull-mounted hydrokinetic turbines (retractable propeller-generators on racing yachts yield a few hundred watts at cruising speeds). Authors in [6] achieved high efficiency at low flow rates with an optimized Archimedes screw turbine. These findings highlight the need to tailor turbine designs to typical yacht speeds (5–10 kn) and make them retractable, as non-retractable units can impose ~9% extra drag.

Authors in [7] optimized a 0.5 m horizontal-axis turbine, yielding ~0.8–0.9 kW at typical speeds. Authors in [8] demonstrated that controllable-pitch propellers can recover energy with minimal thrust loss. Authors in [9] predicted that a ducted hull generator on a tanker could save ~3.5% fuel. Authors in [10] found that larger controllable-pitch systems increase regeneration efficiency but raise drag. Authors in [11] demonstrated that a folding, variable-pitch propeller (SAIL-POD) works for both propulsion and generation. These studies confirm that hydro-generation is feasible and underscore the efficiency–drag trade-offs central to this work.

Authors in [12] noted that optimization methods, such as genetic or surrogate-assisted algorithms, can raise propeller efficiency by 10-13%, but practical design must balance cavitation, vibration, and noise. Enlarging the blade area or modifying the tips may improve efficiency. However, it may alter cavitation and acoustic behavior. Thus, regenerative propellers require evaluation not only for energy yield but also for cavitation risk and structural integrity. Despite the progress, key gaps remain: few studies characterize the integrated hydrodynamic performance with regenerative turbines under realistic conditions. Most, such as [13], analyzed turbine or propeller designs in isolation or simulated narrow scenarios without quantifying the effects on resistance, speed, or seakeeping. The literature lacks a holistic framework coupling turbine operation with yacht hydrodynamics, linking drag, stability, and energy yield. No high-fidelity study has yet provided such integration or clear design guidelines to minimize drag while enabling useful regeneration. Bridging this gap is vital to transition regenerative hydro-turbines from theoretical to practical, performance-optimized systems.

The push for sustainable ship propulsion has intensified under emission regulations and climate goals. In yachting, "zero-emission" strategies combine electrification with renewable energy. Authors in [14] showed that embedding renewables into commercial vessel systems could significantly reduce emissions, encouraging their adoption in yachts. Authors in [15] extended this by designing a motor-superyacht powered by solar, wind, and hydro power, highlighting the importance of system-level energy management with multiple inputs and storage. Sailing yachts are distinct since they already use renewable wind power for primary propulsion. The challenge shifts to supplying auxiliary power and adapting propulsors for dual-mode use, functioning for both thrust and regeneration.

A central research focus is on propulsors capable of efficient operation in both propulsion and generation. Propellers convert shaft power into thrust, while turbines extract energy from flow, but efficiency in one mode rarely transfers to the other. The dual-mode design process (Figure 1) begins with meeting thrust and power requirements, followed by geometry selection, using series or lifting-line methods, and is refined through computational analysis to confirm performance and cavitation limits. Surrogate-assisted optimization enables multi-objective searches balancing thrust and torque in both directions [4]. Yet, authors in [12] emphasized that nonlinear design spaces and convergence issues limit automation, so practical workflows still combine analytical methods with high-fidelity CFD for verification and fine-tuning.

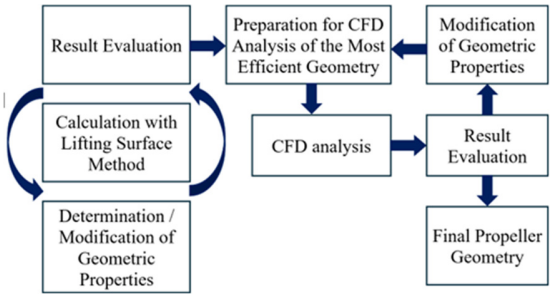

Fig. 1. Propeller design methodology.

Hydrokinetic turbines studied for river and tidal flows provide lessons for yacht use. Authors in [16] designed and validated a three-bladed ocean-current turbine with a power coefficient of ~0.45, confirmed in towing-tank tests. This iterative approach, specifically hydrodynamic optimization followed by prototype trials, demonstrates how small turbines (1–3 m) can be tuned for efficiency, with insights on lift distribution and composite strength directly applicable to yachts. Deployment on sailing craft, however, is complicated by unsteady inflows, hull motions, and the need for retractable systems. Commercial solutions, such as Watt&Sea pod systems, generate several hundred watts at 5–6 kn. Though modest in efficiency, they capture otherwise wasted energy and are valued in long-distance sailing. Given the limited academic data on yacht-specific devices, broader turbine research remains vital as a benchmark.

Advances in propeller wake physics and four-quadrant mapping expose further gaps. Large-eddy simulations resolve wake vortices but seldom quantify drag penalties or energy

recovery when propellers act as turbines [17]. Four-quadrant maps improve motion prediction, yet they remain underutilized in yacht-scale regeneration studies [18]. Dual-mode rotor optimizations exist, but there is scarce guidance on when regeneration yields a net benefit under realistic sailing [19]. The current study addresses these gaps by: (i) generating yacht-scale KT-KQ-J maps including the turbine regime, (ii) embedding these within a validated RANS CFD hull model to quantify ΔR and speed loss, and (iii) producing operating charts that identify "sweet spots", where energy yield outweighs penalties [20].

This study presents a hydrodynamic performance analysis of a sailing yacht with regenerative hydro-turbines, assessing both propulsion and energy generation. The research extends zero-emission yacht studies [1] by focusing on coupled hydrodynamic effects. The contributions are: (A) design of a custom two-bladed, low-speed propeller for minimal power draw; (B) CFD-based evaluation of the propeller performance and of its interaction with hull resistance and turbine drag, and (C) trade-off analysis when turbines are engaged for regeneration. The current study aims to guide naval architects in understanding practical deployment, quantifying penalties in speed and efficiency, and identifying design choices to mitigate them.

Regeneration must also be framed within overall vessel performance. The International Windship Association shows that wind-assist devices can reduce fuel use significantly and that pairing with energy-recovery systems enhances energy balance [21]. At the yacht scale, renewables typically combine solar, wind, and hydrogeneration. Authors in [22] emphasized the variability but abundance of marine renewables, suggesting vessels as platforms for energy harvesting. The present work builds on this perspective, quantifying drag and energy production from yacht-mounted turbines and evaluating propeller design strategies to mitigate losses. This approach provides a yacht-scale case study of integrated regenerative design and performance.

II. METHOD

A. Vessel and Propulsion System

The case study vessel is a 12.5 m sailing yacht, originally powered by a 41.9 kW diesel engine driving a three-bladed, 533 mm propeller through a sail drive with a 2.49:1 reduction (Figure 2). In this baseline configuration, the yacht reaches 6.3 kn at 1500 rpm (≈6 kW delivered) and 7.0 kn at 2100 rpm. For the zero-emission redesign, the diesel and sail drive were replaced by a direct-drive electric pod motor, eliminating the gearbox and improving mechanical efficiency. A 6 kW motor was selected, as it is sufficient for maneuvering, matching the original system's 6.3 kn performance at that power level (Figure 3).

As the new motor operates at 1500 rpm without reduction, a smaller two-bladed propeller was specified to absorb the available power and deliver the target thrust. The design requirements were set as ~1500 N thrust at 6 kn with 6 kW input, while keeping shaft torque within ~38 N·m at 1500 rpm, identified as the critical limit for the motor.

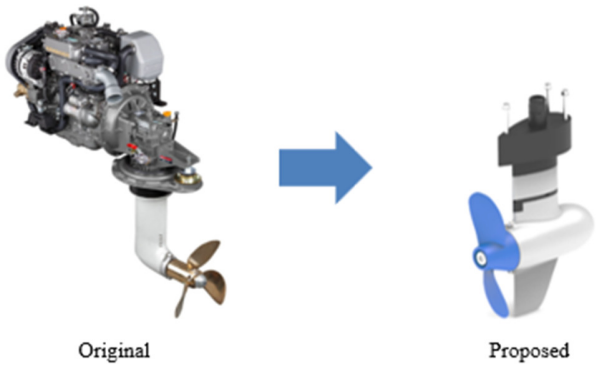

Fig. 2. Original and proposed propulsion system.

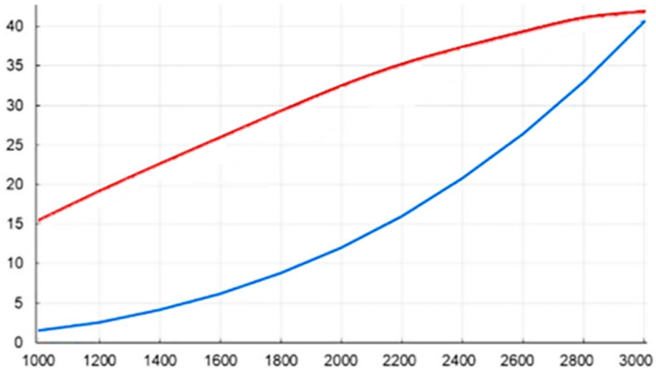

Fig. 3. Performance graph of the case study vessel (kW vs rpm).

B. Propeller Design Procedure

The initial design was derived from the Wageningen B-series, a systematic propeller family suited for preliminary sizing. A two-bladed, 0.34 m diameter configuration was selected for its lower drag in free-wheeling operation and simplified characteristics. Using a lifting-line design tool, the pitch and blade area were iteratively tuned to meet the thrust and power coefficient requirements at the design point (1500 rpm, advance speed ≈3 m/s, 6 kn). Subsequent refinement with a lifting-surface method adjusted radial pitch and section geometry to maximize efficiency while remaining within cavitation limits. The optimized geometry yielded an Expanded Area Ratio (EAR) of ~0.22 and a mean pitch ratio of ~0.67, producing a narrow-bladed propeller with moderate pitch (Table I). Sections were based on NACA profiles, reinforced near the root for strength. Both skew and rake were minimized ($\approx 0^\circ$), thereby reducing the vibratory excitation, typically associated with higher-blade-count propellers.

Figure 3 presents the original engine performance curve, which established the 6 kW design point. The two-bladed propeller is mounted directly on the motor shaft within a streamlined pod, with two auxiliary hydro-turbines positioned on the port and starboard sides for deployment under sail and for feathering when not required.

TABLE I. PROPELLER DESIGN PARAMETERS

Property	Value	Unit
Number of blades	2	[-]
Propeller diameter	0.34	[m]
Hub diameter	0.08	[m]
EAR	0.22	[-]
Mean pitch	0.226	[m]
Mean pitch ratio	0.666	[-]

Following the baseline definition, a computational optimization loop was implemented. Open-water CFD simulations were performed across a range of advance ratios (J) to evaluate thrust (T), torque (Q), and open-water efficiency (η_o). Geometry was iteratively modified, principally through incremental changes in pitch and camber distribution, until performance converged toward the design targets.

The optimized propeller achieved an efficiency of ~54% at the 6 kn design condition, representing an improvement over the original three-bladed unit (≈45% efficiency, estimated from series data). This gain demonstrates the advantage of reducing the blade area and optimizing the section distribution for low-power electric drive applications.

Figure 4 presents the final 3D propeller geometry, while Figure 5 shows the two-dimensional blade projection. Non-dimensional radial distributions of chord (c/D), pitch (P/D), and other sectional parameters are summarized in Table II, providing a reproducible reference for future comparative studies.

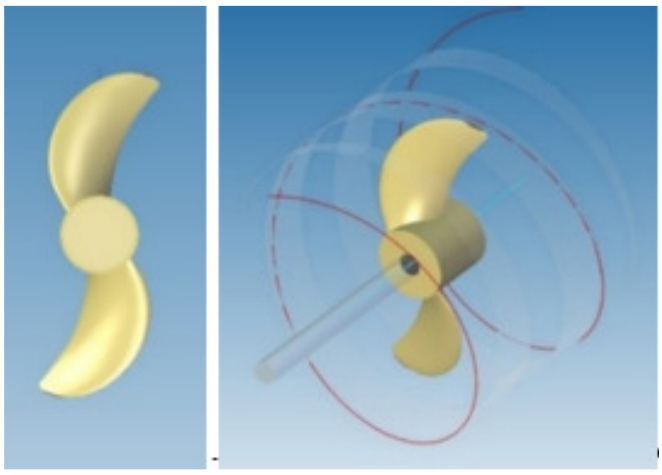

Fig. 4. 3D View of the designed propeller.

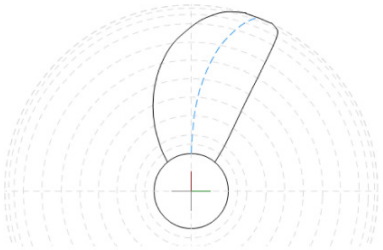

Fig. 5. Propeller blade profile (2D projection).

TABLE II. BLADE GEOMETRY PARAMETERS

r/R	c/D	f_{max}/c	T_{max}/c	$skew^o$	rLe/c
0.2	64.75	2.69	12.53	-18.46	1.34
0.3	68.96	2.93	11.79	-19.89	1.11
0.4	76.15	3.41	9.99	-20.92	0.72
0.5	81.42	3.77	8.32	-19.57	0.47
0.6	84.44	3.71	6.77	-15.08	0.30
0.7	84.59	3.05	5.36	-6.97	0.19
0.8	80.26	2.21	4.13	5.51	0.12
0.9	67.68	1.37	3.14	22.75	0.08
0.95	56.58	0.96	2.42	34.49	0.06
0.98	44.46	0.72	1.96	42.33	0.05
1	22.59	0.53	1.72	48.09	0.07

In Table II, r/R is the sectional radius ratio, c/D is the ratio of chord length to propeller diameter, f_{max}/c is the ratio of maximum camber to chord length, T_{max}/c is the ratio of maximum thickness to chord length, $skew^0$ is the angular skew of the section (angle of the section's midpoint relative to the reference axis), and rLe/c is the ratio of leading-edge radius to chord length.

A two-blade geometry was selected to minimize windmilling drag and simplify folding/feathering while meeting thrust at low shaft power. Electric drive smoothness and light loading mitigated typical 2-blade vibration concerns, and the CFD/FEM-coupled studies showed that composite lay-ups can be tuned to maintain stiffness and suppress adverse modes in slender blades. Increasing propulsive disc area can further lift efficiency. The diameter was ultimately limited by clearance constraints.

C. CFD Setup and Propeller Analysis

The hydrodynamic performance of the propeller and turbines was evaluated using RANS CFD with a rotating reference frame to resolve the flow at moderate shaft speeds. The computational domain was a cylindrical control volume extending ~5 diameters upstream, ~10 diameters downstream, and 5 diameters radially, ensuring negligible blockage effects. Although a two-blade geometry permits 180° periodicity, the influence of strut, pod, and turbines required a full 360° domain for consistency (Figure 6).

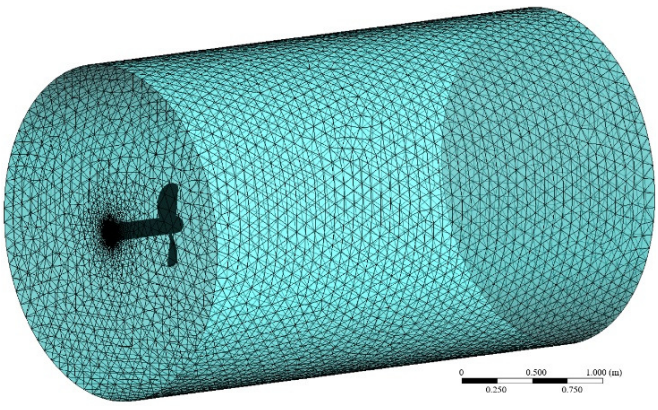

Fig. 6. CFD flow domain and mesh structure.

A hybrid mesh with prism layers along walls and tetrahedral elements in the bulk flow provided a balance

between accuracy and cost. Refinement was concentrated in the slipstream and trailing-edge regions to capture vortex roll-up. The final grids contained several million cells. Convergence studies up to 5 million showed thrust variations <1%. Mesh quality was acceptable (skewness <0.25, $y^+ \approx 50$), confirming its adequacy for full-scale analysis (Figure 7).

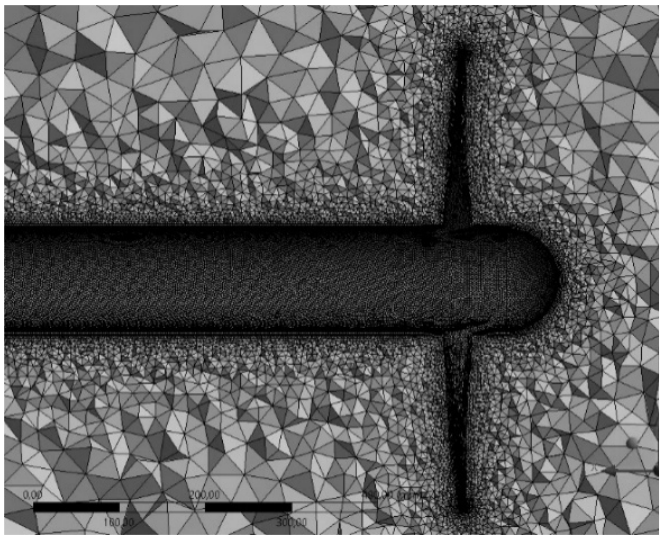

Fig. 7. Mesh cross-section.

The boundary conditions for the open-water propeller tests were: uniform inflow at the inlet, pressure outlet, no-slip on solid surfaces, and slip at the outer boundary. The SST k–ω turbulence model was applied, with water treated as incompressible (ρ = 1025 kg/m³, $\mu = 1.0\times10^{-3}$ Pa·s). Spatial discretization used second-order schemes; all runs converged with residuals reduced by three orders, and transient checks excluded unresolved oscillations. Simulations were conducted over a range of advance ratios ($J = V_A/nD$), with velocity spanning 0–6 kn at rotation rates of 750–1500 rpm. From these, thrust and torque were processed into non-dimensional coefficients:

$$K_T = \frac{T}{\left(\rho n^2 D^4\right)} \quad (1)$$

$$K_Q = \frac{Q}{\left(\rho n^2 D^5\right)} \quad (2)$$

$$\eta_0 = \frac{J}{2\pi} \bullet \frac{K_T}{K_Q} \quad (3)$$

where K_T is the thrust coefficient, K_Q is the torque coefficient, η_0 is the open-water efficiency, T is the thrust (N), Q torque (N m), ρ water density (kg/m^3), n shaft speed (rev/s), D diameter (m), and V_A inflow velocity.

Post-processing included examination of pressure and velocity fields for separation and cavitation risks. Iterative pitch adjustments were introduced when thrust fell below target, refining geometry until requirements were met within torque limits (as presented in Table III and Figure 10). At the design point (1500 rpm, 6 kn), the propeller delivered ~1025 N thrust and ~38 N·m torque, achieving ~54% open-water efficiency versus ~45% for the stock propeller. This performance sustains ~6 kn under electric drive, matches diesel capability, and validates the redesign for zero-emission propulsion.

TABLE III. FLUID ANALYSIS RESULTS

RPM	Speed (kn)	Thrust [N]	Torque [Nm]	μ0 [%]	J	$10K_Q$	K_T
1500	1	1495	53	9.2	0.061	0.174	0.0182
	2	1419	50	18.6	0.121	0.166	0.0172
	3	1347	48	27.6	0.182	0.157	0.0165
	4	1250	45	36.4	0.242	0.146	0.0154
	5	1142	42	44.5	0.303	0.133	0.0144
	6	1025	38	54	0.363	0.12	0.013
1250	1	1097	37	11.7	0.073	0.184	0.0183
	2	1013	35	22.7	0.145	0.17	0.0173
	3	917	32	33.8	0.218	0.154	0.0158
	4	823	29	44.6	0.291	0.138	0.0143
	5	686	26	51.8	0.363	0.115	0.0129
	6	579	23	59.4	0.436	0.097	0.0114
1000	1	707	23	15.1	0.091	0.186	0.0178
	2	630	21	29.5	0.182	0.165	0.0162
	3	521	19	40.4	0.272	0.137	0.0147
	4	439	17	50.7	0.363	0.115	0.0131
	5	354	15	58	0.454	0.093	0.0116
	6	265	12	65.1	0.545	0.07	0.0093
750	1	365	12	19.9	0.121	0.17	0.0165
	2	307	11	36.6	0.242	0.143	0.0151
	3	247	9	53.9	0.363	0.115	0.0124
	4	182	8	59.6	0.484	0.085	0.011
	5	115	6	62.8	0.605	0.054	0.0082
	6	43	4	42.2	0.726	0.02	0.0055

D. Turbine Drag and Resistance Simulations

The hydrodynamic penalty of two regenerative turbines was quantified through resistance simulations. When stowed, turbines were assumed to be feathered or folded for minimum drag. Bare-hull resistance and hull-plus-turbine resistance were obtained via CFD, supplemented by foil-drag estimates. The results (Table IV) show that at 6 kn the boat's resistance rose from ~965 N to ~1053 N, an increase of 9.1%. Across 1–7 kn, added resistance consistently remained ~9–10%, typical for small appendages. The total resistance and the relative penalty are given by:

$$R_{total}(V) = R_{hull}(V) + R_{turbines}(V) \quad (4)$$

$$\Delta R(\%) = \frac{R_{total}(V) + R_{HULL}(V)}{R_{hull}(V)} \times 100 \quad (5)$$

When deployed for energy recovery, turbine drag exceeds the stowed condition but is partially offset by generated power. High-fidelity CFD of rotating turbines was outside this study. Instead, drag increments were coupled with assumed turbine efficiencies to estimate the net yields and voyage-level trade-offs, discussed in the Results.

TABLE IV. FLOW ANALYSIS RESULTS

Speed [kn]	Turbine drag [N]	Hull resistance [N]	Hull & turbines [N]	Increase [%]
1	1.3	26.6	29.3	10,14
2	5.4	114.3	125.2	9,48
3	11.7	248.8	272.2	9,42
4	20.3	439.1	479.6	9,23
5	31.0	675.2	737.3	9,19
6	44.0	964.8	1052.9	9,13
7	59.3	1293.6	1412.2	9,17

E. Four Quadrant Mapping and Electrical Power

The propeller was mapped across all four hydrodynamic quadrants to characterize both propulsion and regeneration. This method, widely used in advanced propeller research, evaluates thrust and torque across a full range of advance ratios, including turbine states where thrust becomes negative. In regeneration, the propeller functions as a turbine, extracting energy from vessel motion. Comparable CFD studies [23] of tidal turbines report power coefficients above 0.4 at optimal tip-speed ratios (TSR ≈ 5 for ~1 m/s flows), providing an upper benchmark for yacht-scale regeneration. Mapping, thus, reveals how closely the yacht's propulsor approaches such efficiencies and at what speeds regeneration is the most effective.

The calculations for K_T, K_Q, and J are given above, with the open-water efficiency (η_0) being determined from them. In regeneration, the sign of K_T becomes negative (drag force) and torque reverses, producing electrical power through the motor-generator. For these cases, the available hydrodynamic power and the electrical output are expressed by:

$$P_{hyd} = Q \cdot 2\pi n \quad (6)$$

$$P_{el} = \eta_{gen} \cdot P_{hyd} \quad (7)$$

where η_{gen} is typically 0.8-0.9 for permanent-magnet machines.

The K_T-K_Q-J curves were extended into the turbine regime by allowing negative shaft power. A two-stage approach combined lifting-surface mapping for dense coverage with RANS CFD verification at selected operating points using the k-ω SST model. Mesh independence was confirmed in the tip-vortex and the near-wake regions. Regeneration was further quantified using the electrical power coefficient and a Net Energy Index given by:

$$C_{P,e} = \frac{P_e}{\frac{1}{2}\rho V^3 A'} \quad (8)$$

$$NEI = \frac{P_e}{R_{total} \cdot V} \quad (9)$$

The *NEI* balances the energy harvested against resistance. Contour maps of $C_{P,e,}$ and *NEI* identified "sweet spots", where yield is high and speed loss is modest.

The four-quadrant framework, thus, provides both design and operational value. For naval architects, the K_T-K_Q-J surfaces support motor and controller sizing. For operators, *NEI* contours give practical guidance on when to engage or feather devices, linking hydrodynamics to voyage-level energy budgets. In broader terms, yacht-scale maps serve as performance charts analogous to aero-engine maps, enabling system optimization, control strategy development, and hybrid propulsion planning [18, 19].

III. RESULTS

A. Hydrodynamic Effects

1) Open-Water Propeller Performance

Figure 8 shows the thrust and resistance curves for the two-bladed propeller, with their values summarized in Table III. At the design point (1500 rpm, ~6 kn), the propeller delivers ~1025 N thrust and 38 N·m torque, close to the target 1500 N at 6 kW (39 N·m). The shortfall (~470 N) corresponds to ~5.5 - 6 kn, sufficient for normal cruising. For a higher demand, the motor can reach ~2000 rpm, producing >1300 N thrust and speeds above 7 kn - matching or exceeding the original diesel system. Thus, the electric direct-drive with a smaller two-blade propeller achieves comparable capability while improving efficiency in the primary regime.

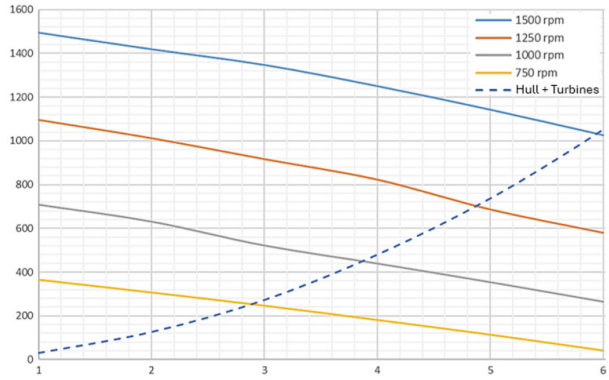

Fig. 8. Propeller thrust and hull resistance (N) curves versus speed (knots).

Efficiency peaks at ~56% near $J \approx 0.8$ (slightly above the design $J \approx 0.12$ at 6 kn, 1500 rpm). At the design point, efficiency is ~54%, compared with ~45% for the original three-bladed unit. Gains stem from the optimized blade geometry and lower load coefficients. Non-dimensional coefficients (K_T, K_Q) across speeds are listed in Table III. As expected, higher advance ratios reduce K_T and K_Q, but raise η_0, until thrust diminishes at a high J. For instance, at 1500 rpm, advancing from 1 to 6 kn lowers K_T from 0.0182 to 0.0130 while raising η_0 from ~9% to ~54%, consistent with open-water behavior.

Figures 9 and 10 illustrate CFD-predicted fields at 1500 rpm, 6 kn. The wake shows a coherent slipstream with axial velocities ~1.2 times free stream, while pressure peaks reach $+1.5\times10^5$ Pa at the leading-edge root and minima of approximately -0.5×10^5 Pa mid-span. No areas approach vapor pressure, confirming cavitation-free operation under design conditions. The simulations assume 1 atm ambient pressure and seawater at 15 °C. Cavitation was screened via $C_{p,min}$, relative to vapor pressure, without a dedicated cavitation model. At higher rpm or in seaways, limited cavitation may occur. This

off-design risk is consistent with the small-propeller hydro-acoustic findings in [24] and motivates this proposed operating envelope.

Overall, the propeller provides the required thrust with ~6 kW input, sustaining ~6 kn and matching the diesel baseline. The design ensures adequate bollard pull for docking and safe cruising. Figure 10 further shows the thrust-resistance intercept at ~6 kn (1500 rpm) and ~5 kn (1250 rpm), aligning with the expectations.

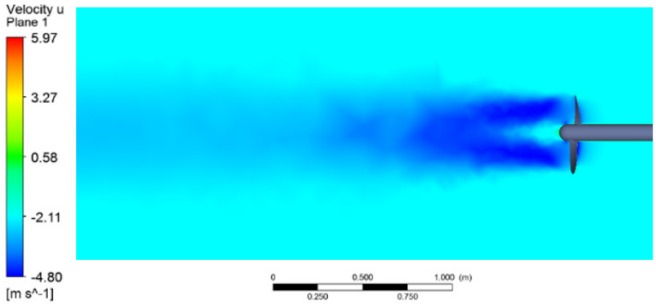

Fig. 9. Wake velocity distribution.

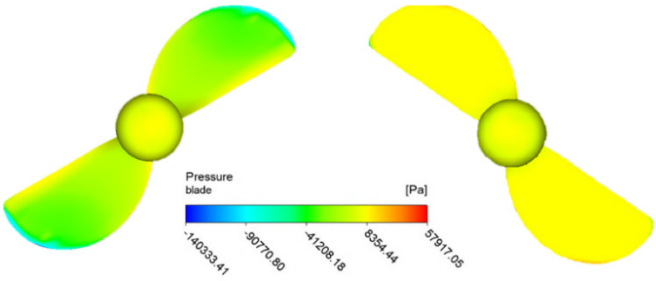

Fig. 10. Blade pressure distribution.

2) Hull Resistance and Turbine Drag

Table IV summarizes resistance with and without stowed turbines. At 5 kn, bare-hull resistance is ~675 N, rising to ~737 N with turbines (9.2% increase). Across 1–7 kn, penalties remain ~9–10%, reflecting drag scaling with speed². Practically, this equates to ~9% lower sailing speed for a given sail thrust or slightly higher motor demand, which is an acceptable cost for regeneration capability.

When the turbines are deployed, drag increases further as the blades generate torque and vortices. For efficient turbines, most of the added drag converts directly into shaft power: $P = T_{turbine} \times V$.

At 5 kn, 1 kW requires ~390 N drag, which is over half the bare-hull resistance, causing a significant slowdown unless additional sail force is available. Hence, regeneration has practical limits: excessive loading stalls the yacht until output falls [4]. The simulations confirm that moderate recovery (0.5–1.0 kW at cruising speeds) is feasible without compromising performance. In this design, each turbine typically operates at 200–300 N drag, yielding 200–300 W at an approximately 20–30% efficiency. Though modest, continuous charging can meaningfully extend sailing autonomy.

IV. DISCUSSION AND CONCLUSIONS

This study assessed the hydrodynamic and regenerative performance of a sailing yacht equipped with a custom propeller and auxiliary hydro-turbines, offering valuable insights for naval architects and marine engineers pursuing zero-emission yacht design. The two-bladed, 0.34 m propeller achieved ~54% open-water efficiency at 6 kn and 6 kW input, producing ~1.0 kN thrust at 1500 rpm, compared to the original 41 kW diesel system. The efficiency gains over the stock three-blade (~45%) confirm that systematic design, Computational Fluid Dynamics (CFD) verification, and optimized blade geometry can deliver substantial improvements. Although two-bladed propellers are often avoided due to vibration, the electric drive's smooth torque and light loading mitigated this concern. Prior research [25] indicates that further efficiency gains may be achieved by enlarging the disk area and tailoring composite lay-ups via CFD/FEM coupling to balance hydrodynamic and structural performance [26].

Integrating hydro-turbines introduces a direct trade-off between energy capture and added drag. Stowed turbines increased resistance by ~9-10% across 3-7 kn, consistent with the expectations for small appendages. When generating, each unit produced several hundred watts at 5-6 kn, with vessel slowdown limited to ~0.3-0.5 kn. At higher loads (multi-kW), drag penalties rose sharply. These findings align with [27], which emphasized that the value of hydro-turbines depends not only on instantaneous efficiency but also on how regeneration interacts with vessel mission profiles and environmental conditions. Adaptive deployment strategies are, therefore, critical, with energy management systems optimizing regeneration without unduly compromising sailing performance. Variable-pitch and reversible propeller concepts [4] offer further efficiency potential, though they add mechanical complexity.

Several design levers exist to improve the energy-to-drag ratio. Controllable-pitch or dual-mode geometries can keep operation near four-quadrant "sweet spots" [28], compact diffusers or shrouds may enhance power extraction [29], and flow-conditioning devices, such as blocking plates, have demonstrated ~10–18% improvements in laboratory turbine tests [30]. Authors in [11] further highlight the importance of wake stability and hydroacoustics in off-design operation. Collectively, these strategies point toward incremental but meaningful performance gains that could make yacht-scale regeneration more effective.

This study prioritized hydrodynamic feasibility, confirming that propulsion efficiency and maneuverability were preserved. From an energy-centric viewpoint, every watt recovered must be weighed against knots lost, reframing the design as a cost–benefit trade-off. For cruising yachts, autonomy and freedom from shore power often outweigh small speed losses, as scenario simulations confirmed [1]. For racing, regeneration can simply be deactivated. The dual-mode system, thus, offers operational flexibility, maximizing recovery during surplus wind and minimizing penalties when speed matters.

Alternative zero-emission concepts, such as hydrogen fuel cells, solar-only systems, and towed generators, face drawbacks

related to cost, autonomy, or reliability. In contrast, integrating regeneration into existing appendages combines practicality with efficiency, reviving a century-old concept now made viable by advanced materials and modern CFD tools.

The findings confirm that regenerative propulsion is feasible for small craft as long as it is approached holistically, with propellers designed for both thrust and torque harvesting. Podded drives ease integration and reduce penalties. Future work should extend to unsteady conditions (waves, heel, off-axis inflow) via either towing-tank or unsteady CFD validation. Intelligent control, potentially machine-learning-based, could optimize deployment in real time, while feathering or variable-pitch propellers offer improved capture. Lifecycle and economic analyses will further quantify long-term savings.

In summary, regenerative hydro-turbines can be implemented with modest performance losses and substantial renewable gains. The present study merged classical naval architecture with modern energy technology, offering a validated pathway toward sustainable and zero-emission yacht design [31, 32].

ACKNOWLEDGMENT

The authors gratefully acknowledge the support provided by Istanbul Technical University.

REFERENCES

[1] H. S. Nomak and İ. Çiçek, "Yenilenebilir Enerji Kaynakları ile Sıfır Emisyonlu bir Yelkenli Tekne Tasarımı ve Seyir Simülasyonları," *Çevre İklim ve Sürdürülebilirlik*, vol. 23, no. 1, pp. 41–54, May 2022.

[2] E. V. Palconit and M. L. S. Abundo, "Transitioning to green maritime transportation in Philippines : mapping of potential sites for electric ferry operations," *Engineering, Technology & Applied Science Research*, vol. 9, no. 1, pp. 3770-3773, 2019.

[3] R. C. Matthews, L. J. Rashkin, S. F. Glover, and N. H. Doerry, "Stabilization of Generator Frequency Under Pulsed Load Condition Using Regenerative Propeller Braking," *in 2021 IEEE Electric Ship Technologies Symposium (ESTS)*, Arlington, VA, USA, Aug. 2021, pp. 1–6, https://doi.org/10.1109/ESTS49166.2021.9512335.

[4] L. Van Heugten, "A surrogate-assisted propeller optimisation in propulsive and regenerative operations," *Delfth University of Technology*, July 2023.

[5] A. Ali et al., "Small hydropower generation using pump as turbine; a smart solution for the development of Pakistan's energy," *Heliyon*, vol. 9, no. 4, 2023, Art. no. e14993, https://doi.org/10.1016/j.heliyon.2023.e14993.

[6] M. Zamani, R. Shafaghat, and B. Alizadeh Kharkeshi, "Numerical Study of the Hydrodynamic Behavior of an Archimedes Screw Turbine by Experimental Data in order to Optimize Turbine Performance: The Genetic Algorithm," *Journal of Applied and Computational Mechanics,* vol. 9, no. 4, pp. 1060–1075, 2023, https://doi.org/10.22055/jacm.2023.43137.4031.

[7] S. Ekinci and M. Alvar, "Horizontal Axis Marine Current Turbine Design for Wind-Electric Hybrid Sailing Boat," *Brodogradnja : An International Journal of Naval Architecture and Ocean Engineering for Research and Development*, vol. 68, no. 2, pp. 127–151, 2017, https://doi.org/10.21278/brod68209.

[8] P. Liu, N. Bose, K. Chen, and Y. Xu, "Development and optimization of dual-mode propellers for renewable energy," *Renewable Energy*, vol. 119, pp. 566–576, Apr. 2018, https://doi.org/10.1016/j.renene.2017.12.041.

[9] W. Yutuc, "Use of Hydro Generator on a Tanker Ship: A Computer-Generated Simulation Study," *in Computational Science and Its Applications – ICCSA 2013*, Berlin, Heidelberg, 2013, pp. 207–219, https://doi.org/10.1007/978-3-642-39643-4_16.

[10] M. Van der Plas, W. Hullege, and P. De Vos, "The impact of hydro generation on board large sailing yachts," *in Proceedings of 15th International Marine Design Conference (IMDC-2024)*, Amsterdam, Netherlands, June 2024, https://doi.org/10.59490/imdc.2024.906.

[11] D. Calcagni, A. Mancini, and R. Baffigo, "Innovative dual-function SAIL-POD by Velettrica: experimental assessment and performance calibration," *Journal of Marine Science and Technology*, vol. 30, no. 2, pp. 392–407, June 2025, https://doi.org/10.1007/s00773-025-01057-z.

[12] B. Bacalja Bašić, M. Krčum, and Z. Jurić, "Propeller Optimization in Marine Power Systems: Exploring Its Contribution and Correlation with Renewable Energy Solutions," *Journal of Marine Science and Engineering*, vol. 12, no. 5, May 2024, Art. no. 843, https://doi.org/10.3390/jmse12050843.

[13] E. Julià, F. Tillig, and J. W. Ringsberg, "Concept Design and Performance Evaluation of a Fossil-Free Operated Cargo Ship with Unlimited Range," *Sustainability*, vol. 12, no. 16, Aug. 2020, Art. no. 6609, https://doi.org/10.3390/su12166609.

[14] G. Minak, "Solar Energy-Powered Boats: State of the Art and Perspectives," *Journal of Marine Science and Engineering*, vol. 11, no. 8, 2023, Art. no. 1519, https://doi.org/10.3390/jmse11081519.

[15] E. Eastlack et al., "Zero Emission Super-Yacht," *in 2019 Fourteenth International Conference on Ecological Vehicles and Renewable Energies (EVER)*, Monte-Carlo, Monaco, May 2019, pp. 1–8, https://doi.org/10.1109/EVER.2019.8813677.

[16] Sadeqi, "Blade Design and Validation of Hydrokinetic Turbine to Harvest Water Current Energy," *University of New Orleans*, 2024.

[17] Z. Zhang, P. Sun, L. Pan, and T. Zhao, "On the propeller wake evolution using large eddy simulations and physics-informed space-time decomposition," *Brodogradnja : An International Journal of Naval Architecture and Ocean Engineering for Research and Development*, vol. 75, no. 1, pp. 1–21, 2024, https://doi.org/10.21278/brod75102.

[18] T. Cosgun, M. Esenkalan, and O. K. Kinaci, "Four-quadrant propeller hydrodynamic performance mapping for improving ship motion predictions," *Brodogradnja : An International Journal of Naval Architecture and Ocean Engineering for Research and Development*, vol. 75, no. 3, pp. 1–20, 2024, Art. no. 75306, https://doi.org/10.21278/brod75306.

[19] J. R. Erriah, P. Liu, and S. Turkmen, "Hydrodynamic Development and Optimisation of a Retrofittable Dual-Mode Propeller Turbine," *Energies*, vol. 17, no. 13, June 2024, Art. no. 3138, https://doi.org/10.3390/en17133138.

[20] Z. Ma, N. Ji, Q. Zeng, X. Deng, and C. Shi, "Influence of scale effect on flow field offset for ships in confined waters," *Brodogradnja : An International Journal of Naval Architecture and Ocean Engineering for Research and Development*, vol. 75, no. 1, pp. 1–22, 2024, https://doi.org/10.21278/brod75106.

[21] "2023 IMO Strategy on Reduction of GHG Emissions from Ships," *International Maritime Organization*, https://www.imo.org/en/ourwork/environment/pages/2023-imo-strategy-on-reduction-of-ghg-emissions-from-ships.aspx.

[22] C. Chen, C. Peng, H. Xiao, T. Wang, and M. Wei, "Numerical Distribution Simulation of Typhoons' Wave Energy in the Taiwan Strait and its Adjacent Waters," *Brodogradnja : An International Journal of Naval Architecture and Ocean Engineering for Research and Development*, vol. 73, no. 4, pp. 39–52, 2022, https://doi.org/10.21278/brod73403.

[23] A. C. Loh, O. Yongson, L. Samylingam, D. Rilling, C. K. Kok, and G. M. Chen, "CFD analysis of Hydrodynamic Characteristics of Tidal Current Turbines," *Engineering, Technology & Applied Science Research*, vol. 15, no. 2, pp. 22049–22058, Apr. 2025, https://doi.org/10.48084/etasr.9293.

[24] E. J. Yeo, D. M. Kennedy, and F. O'Rourke, "Tidal current turbine blade optimisation with improved blade element momentum theory and a non-dominated sorting genetic algorithm," *Energy*, vol. 250, July 2022, Art. no. 123720, https://doi.org/10.1016/j.energy.2022.123720.

[25] A. Sánchez-Caja, J. Martio, and V. M. Viitanen, "A new propulsion concept for high propulsive hydrodynamic efficiency," *Ocean Engineering*, vol. 243, Jan. 2022, Art. no. 110298, https://doi.org/10.1016/j.oceaneng.2021.110298.

[26] L. Liang, Z. Baoji, Z. Hao, T. Hailin, and W. Weijie, "Hydrodynamic performance optimization of marine propellers based on fluid-structure coupling," *Brodogradnja : An International Journal of Naval Architecture and Ocean Engineering for Research and Development*, vol. 74, no. 3, pp. 145–164, June 2023, https://doi.org/10.21278/brod74308.

[27] Q. Sun, W. Qi, H. Liu, X. Ji, and H. Qian, "Toward Long-Term Sailing Robots: State of the Art From Energy Perspectives," *Frontiers in Robotics and AI*, vol. 8, Jan. 2022, https://doi.org/10.3389/frobt.2021.787253.

[28] T. K. Das, Z. Sun, C. Li, M. Tadros, and W. Shi, "Hydrodynamic performance of a ducted controllable pitch propeller with wavy leading edge," *Ocean Engineering*, vol. 331, July 2025, Art. no. 121349, https://doi.org/10.1016/j.oceaneng.2025.121349.

[29] C. Y. Ng, N. R. Maldar, and M. C. Ong, "Numerical investigation on performance enhancement in a drag-based hydrokinetic turbine with a diffuser," *Ocean Engineering*, vol. 298, Apr. 2024, Art. no. 117179, https://doi.org/10.1016/j.oceaneng.2024.117179.

[30] V. Patel, V. Rathod, and C. Patel, "Optimal utilization of hydrokinetic energy resources through performance improvement of the darrieus turbine using concave and flat blocking plates," *Ocean Engineering*, vol. 283, Sept. 2023, Art. no. 115099, https://doi.org/10.1016/j.oceaneng.2023.115099.

[31] Z. Cheng, B. Smoker, S. Kashyap, G. Burella, and R. K. Jaiman, "Cavitating wake dynamics and hydroacoustics performance of marine propeller with a nozzle," *Physics of Fluids*, vol. 37, no. 1, Jan. 2025, Art. no. 015128, https://doi.org/10.1063/5.0247891.

[32] M.-R. Pendar and P. Oshkai, "High-fidelity modeling of cavitating flow around a marine propeller with bio-inspired wavy rudder configurations: Radiated noise analysis using hydro-acoustic analogies," *Physics of Fluids*, vol. 37, no. 3, Mar. 2025, Art. no. 033375, https://doi.org/10.1063/5.0257316.